Inorganic Chemistry
Article
Cite This: Inorg. Chem. 2018, 57, 8078−8088
pubs.acs.org/IC

Unusual Reduction Mechanism of Copper in Cysteine-Rich Environment

Biplab K. Maiti, Luisa B. Maia, Artur J. Moro, João C. Lima, Cristina M. Cordas, Isabel Moura, and José J. G. Moura*

LAQV, REQUIMTE, Departamento de Química, Faculdade de Ciências e Tecnologia, Universidade Nova de Lisboa, 2829-516 Caparica, Portugal

Supporting Information

ABSTRACT: Copper−cysteine interactions play an important role in Biology and herein we used the copper-substituted rubredoxin (Cu-Rd) from *Desulfovibrio gigas* to gain further insights into the copper-cysteine redox chemistry. EPR spectroscopy results are consistent with Cu-Rd harboring a Cu^{II} center in a sulfur-rich coordination, in a distorted tetrahedral structure ($g_{\|,\perp}$ = 2.183 and 2.032 and $A_{\|,\perp}$ = 76.4 × 10^{-4} and 12 × 10^{-4} cm^{-1}). In Cu-Rd, two oxidation states at Cu-center (Cu^{II} and Cu^{I}) are associated with Cys oxidation−reduction, alternating in the redox cycle, as pointed by electrochemical studies that suggest internal geometry rearrangements associated with the electron transfer processes. The midpoint potential of $[Cu^{I}(S{-}Cys)_2(Cys{-}S{-}S{-}Cys)]/[Cu^{II}(S{-}Cys)_4]$ redox couple was found to be −0.15 V vs NHE showing a large separation of cathodic and anodic peaks potential (ΔE_p = 0.575 V). Interestingly, sulfur-rich Cu^{II}-Rd is highly stable under argon in dark conditions, which is thermodynamically unfavorable to Cu−thiol autoreduction. The reduction of copper and concomitant oxidation of Cys can both undergo two possible pathways: oxidative as well as photochemical. Under O_2, Cu^{II} plays the role of the electron carrier from one Cys to O_2 followed by internal geometry rearrangement at the Cu site, which facilitates reduction at Cu-center to yield $Cu^{I}(S{-}Cys)_2(Cys{-}S{-}S{-}Cys)$. Photoinduced (irradiated at λ_{ex} = 280 nm) reduction of the Cu^{II} center is observed by UV−visible photolysis (above 300 nm all bands disappeared) and tryptophan fluorescence (~335 nm peak enhanced) experiments. In both pathways, geometry reorganization plays an important role in copper reduction yielding an energetically compatible donor−acceptor system. This model system provides unusual stability and redox chemistry rather than the universal Cu−thiol auto redox chemistry in cysteine-rich copper complexes.

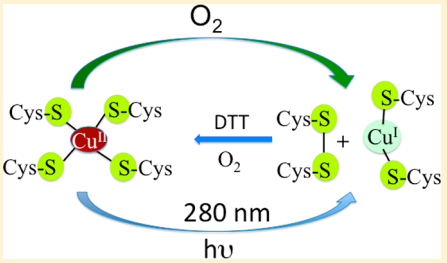

1. INTRODUCTION

Copper−cysteine interactions are present in active sites of many classes of copper-proteins for a wide range of biological processes.[1−3] This interaction arises from the redox-active nature of both copper and thiol, resulting in the formation of a versatile and unusual coordination species such as Cu^{I} with terminal or bridging thiolates,[4−6] Cu^{I} with bridging disulfides,[7] mixed-valent Cu^{I}, Cu^{II} with bridging thiolates,[8] and Cu^{II} with terminal or bridging thiolates.[3] Among these, in biology, highly specific, sulfur-rich copper-proteins (e.g., Atox1, Cox17, Sco1, CCS, metallothioneins) are normally present as Cu^{I} and exist in several metallo-forms with different metal-binding stoichiometry, which actively play safe and efficiently delivering copper ions from their entry in the cell to its final protein incorporation.[4−6,9−12] When reducing the number of thiol (cysteine) coordination to one or two at the copper site, normally mono- and bimetallic copper active sites occur in biological contexts,[2,3,13] and frequently, these are associated with rapid, reversible electron transfer processes shuttling between the cuprous and cupric oxidation states. The mononuclear Cu^{II}-thiolate center is also fascinating to chemists due to their intense Cu^{II}-thiolate electronic absorption features that reflect the covalency of the copper-thiolate bond which make major contributions to reactivity in a variety of copper-containing metalloproteins such as red, blue, and green cupredoxins and in which their functionalities are based on Cu^{II}/Cu^{I} redox processes influenced by the geometry at the copper site.[14−17] Some copper-redox enzymes are involved in sulfur (cysteine)-based redox reactions such as Cox17 and Sco1 proteins which deliver copper to the Cu_A site of CcO through copper thiolate/disulfide redox mechanism (oxidative switch).[8,18,19] These redox conversions are also associated with aging, cancer and neurological disorders such as Alzheimer's disease in the presence of reactive oxygen species (ROS).[20−23] Thus, the control of the oxidation states of copper and sulfur in the resulting products is a major concern in the field of copper−thiolate chemistry.

There is also a challenging problem in the synthesis of sulfur-rich Cu^{II}-thiolate complexes due to the facile redox reaction (thermodynamically favorable) [$2RS^{-}$ + $2Cu^{II}$/RSSR + $2Cu^{I}$], as evidenced in the literature.[24−29] Therefore, it is believed that copper is reduced by thiols, and in excess, these thiols are able to subsequently bind the cuprous ions to generate Cu^{I}−thiol complexes.[25,30]

Received: January 12, 2018
Published: June 29, 2018

DOI: 10.1021/acs.inorgchem.8b00121
Inorg. Chem. 2018, 57, 8078−8088

Overall, the active site of a range of copper-enzymes shows remarkable variation in copper−sulfur coordination, but they do not contain $Cu^{II}S_4$ cores, even in chemically synthesized copper-thiol complexes. The motivation for these studies is the understanding of the inorganic chemistry of a mononuclear $Cu^{II}S_4$ site, which is not found in current known metalloproteins, and it is a difficult endeavor (and perhaps the reason why nature does not seem to produce it) because Cu^{II} is typically reduced by the cysteine thiolate to Cu^{I} with concomitant oxidation of the thiolate to a disulfide (RSSR). Therefore, in order to prepare an artificial intact $[Cu^{II}\text{-}(S{-}Cys)_4]$ center, this has been generated only by replacing Fe^{II} by Cu^{II} in the active site of rubredoxin.[31] Rubredoxin (Rd) is a small (≈6 kDa) nonheme iron electron transfer protein containing a distorted tetrahedral $Fe(S{-}Cys)_4$ site with Fe^{II} or Fe^{III} formal oxidation states that is surrounded by a pair of iron-ligated CXXC (X = amino acid; C = cysteine) loops and have extraordinary resistance to denaturation and metal release.[32] A wide range of metal-substituted derivatives has been studied in order to elucidate the structural and electronic properties of metal sites and these proved to be useful as model systems.[33,34] Among these, Cu^{II}-Rd is coordinated with a pair of Cys loops ($-C_6-XX-C_9-$ and $-C_{39}-XX-C_{42}-$) and the geometry of Cu site is affected during the redox process.[31] Copper-substituted forms of the wild-type Rd were first reported from *Desulfovibrio vulgaris Hildenborough*.[31] Copper uptake, occurring mainly as Cu^{II} species, with cysteine residues in proteins, is believed to reduce Cu^{II} to Cu^{I} with the simultaneous oxidation of thiol to disulfides but the exact nature of the mechanism conducting these internal redox processes still remains unclear.

Herein, we present copper-substituted forms of the recombinant Rd from *Desulfovibrio gigas* showing unusual redox chemistry in cysteine rich copper−thiol interactions. Reduction of copper occurs either by oxidative pathway where O_2 play a role as catalyst or by a photochemical pathway. In both cases, it is shown that geometry plays an important role. In anoxic conditions, copper is also reduced by UV-light (λ_{ex} = 280 nm), which was detected by dark and UV−visible light and tryptophan fluorescence studies. This redox chemistry leads to generation of several reactive intermediates that are also challenging to characterize because of their transient and unstable nature.

2. MATERIALS AND METHODS

2.1. Reagents. All reagents were purchased from Fisher Scientific and Sigma-Aldrich and were used as received unless otherwise noted.

2.2. Expression, Isolation, and Purification of Fe-Rd and Preparation of apo-Rd. *Desulfovibrio gigas* Rd was heterologously expressed in *E. coli* BL21(DE3) as an iron-containing rubredoxin (Fe-Rd),[35] and the protein was purified as previously described.[36,37] The purity of the Fe-Rd was checked by SDS-PAGE and UV−visible spectrum showing an $A_{280\ nm}/A_{494\ nm}$ purity ratio of 2.4. The apo-Rd was also prepared and quantified according to published procedures.[38] After preparation of apo-Rd by acid precipitation (three times to reduce the metal (Fe) content), the precipitate was dissolved in 50 mM Tris-HCl, pH 7.6, buffer, and the solution transferred into a dialysis bag for dialysis over 10−12 h at 4 °C in the same buffer to remove excess DTT and trichloroacetic acid (TCA). The final apo-Rd solution was obtained as disulfide-reduced apo-Rd. The apo-Rd was concentrated up to 4 mM by ultrafiltration (centrifugation) using an YM5 membrane filter (size exclusion of 5 kDa; Sartorius) and kept in −20 °C freeze for further use.

2.3. Preparation of Cu^{II}-Rd Derivatives. CuRd derivatives were prepared by two methods as follows: (1) breaking of the S−S bonds using DTT and (2) reducing S−S bonds using DTT followed by dialysis to remove the DTT. Both experiments are carried out under oxic or anoxic condition.

The first procedure is similar to that in our previous report.[31]

In the second procedure, the disulfide-reduced apo-Rd (reduced by DTT, followed by dialysis) is directly reconstituted with $CuSO_4$ (or $CuCl_2$) with immediately appearance of a brown color due to the high affinity of Cu−thiol interaction. Then, 1 mM of $CuSO_4$ was added into 1 mM of apo-Rd in 2.5 mL of 50 mM Tris-HCl, pH 7.6, under anoxic conditions. The mixture was incubated for 10 min, on an ice bath (4 °C). The protein was quickly passed (to minimize the redox reaction) into a size-exclusion chromatography (PD-10 column; size exclusion of 5 kDa; GE Healthcare) equilibrated with 50 mM Tris-HCl, pH 7.6, and subsequently separated from unbounded metal ions form; and the elution was carried out with the same buffer. The fraction containing the substituted protein was collected and kept in argon and covered to protect it from light. The SDS-PAGE gel of Cu-Rd (without thiol) shows only one band with ∼6 kDa.

UV−visible spectra were collected under anaerobic conditions (or aerobic conditions when mentioned) in septum-sealed 1 cm path-length cuvettes using a Shimadzu UV-1800 spectrophotometer at 22 °C.

2.3.1. Reduction Assay of Cu^{II}-Rd to Cu^{I}-Rd by O_2. The Cu^{II} reduction in Cu^{II}-Rd was performed with oxygen. The experiments were conducted under aerobic conditions where availability of oxygen would allow reduction of copper which was monitored by absorption spectroscopy and where three visible absorption bands uniformly disappear with time, suggesting the formation of Cu^{I}-Rd. In this experiment, 40 μM Cu^{II}-Rd in 1 mL of 50 mM Tris-HCl, pH 7.6, in a 1 cm quartz optical cell, was conducted in air over 7−8 h at RT.

2.3.2. Reduction Assay of Cu^{II}-Rd to Cu^{I} by Addition of Excess Cu^{II} Salt. The Cu^{II} reduction in Cu^{II}-Rd was assayed with excess free $CuSO_4$. For this experiment, 90 or 180 μM of $CuSO_4$ was added into 90 μM Cu^{II}-Rd in 1 mL of 50 mM Tris-HCl, pH 7.6, in a 1 cm quartz optical cell, under strict anoxic or aerobic condition over 2 h at RT.

2.3.3. Reduction Assay of Cu^{II}-Rd to Cu^{I} by Photolysis. The Cu^{II} reduction in Cu^{II}-Rd was assayed by UV−visible light irradiation (λ_{ex} = 280 nm). For this experiment, the 90 μM Cu^{II}-Rd in 1 mL of 50 mM Tris-HCl, pH 7.6, in a 1 cm quartz optical cell, under strict anoxic condition was followed over 30 min at RT. One set of the same sample kept in dark condition (wrap with aluminum foil) at RT for control experiment.

2.3.4. Fluorescence and UV−Visible Assays of Cu-Rd. The same samples (obtained aerobically as well as by photolysis reduction) are used for the assays of UV−visible followed by fluorescence to avoid any manual error.

2.3.5. Recycling of Cu^{I}-Rd to Cu^{II}-Rd by DTT and Presence of O_2. After reduction of copper by aerobic as well as photolysis, both samples are tested for recycle the redox chemistry. Then, 2 mM DTT is added into both samples and experiments are conducted under aerobic conditions where availability of oxygen allow recycling of copper oxidation states which was monitored by regenerating absorption bands over 2−3 h at RT.

2.4. Metal and Protein Quantification. The copper content was determined by inductively coupled plasma (ICP) emission analysis in a Jobin Yvon Ultima instrument using the Reagecom 23 ICP multi-elements as a standard solution, in a concentration range of 0.05−6 ppm. The protein concentration was determined by the Lowry method,[39] using bovine serum albumin (BSA) as standard protein. Cu/Rd = 0.95:1.

2.5. Instrument Description. *2.5.1. UV−Visible Photolysis.* UV/vis absorption spectra were recorded on a Varian Cary 100 Bio or 5000 spectrophotometer. All sample solutions were prepared under argon and the cuvette was closed by a rubber septum immediately prior to photolysis study. The solutions were irradiated in a quartz cuvette (path length = 1 cm) with magnetic stirring, using a 300 W xenon arc-lamp equipped with 280 nm cutoff filter. The absorption spectra were registered before irradiation and at selected time points of irradiation period.

2.5.2. Fluorescence. Emission spectra were acquired on a Horiba-Jobin-Ybon SPEX 159 Fluorolog 3.22, in quartz cuvettes

DOI: 10.1021/acs.inorgchem.8b00121
Inorg. Chem. 2018, 57, 8078−8088

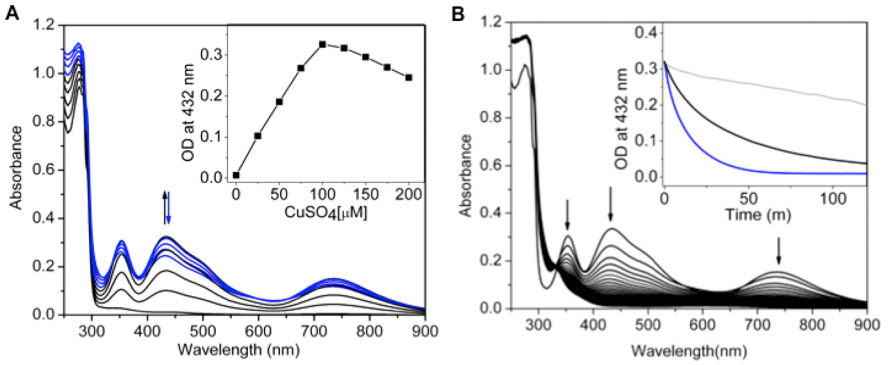

Figure 1. (A) UV−vis spectra of apo-Rd (≈90 μM) with $CuSO_4$ (black lines; 0, 25, 50, 75, and 100 μM $CuSO_4$. blue lines; 125, 150, 175, and 200 μM $CuSO_4$; total titration time 8−10 min) in Tris-HCl buffer, pH 7.6, at RT. Inset: OD at 432 nm vs $CuSO_4$ addition. (B) UV−visible of Cu^{II}-Rd (≈90 μM) with 2 equiv (≈180 μM) of $CuSO_4$ decays with time over 2 h every 2 min in Tris-HCl buffer, pH 7.6, at RT. Inset: Comparison decay rate, OD at 432 nm vs time (over 2 h) (gray: 0 equiv of $CuSO_4$, black: 1 equiv of $CuSO_4$ and blue: 2 equiv of $CuSO_4$). Arrows indicate the directions.

(path length = 1 cm), with excitation and emission slit widths set to 1 nm and an integration time of 0.1s.

2.5.3. Electrochemical Studies. Cyclic voltammetry (CV) was performed, at RT, using a potentiostat/galvanostat AUTOLAB PGSTAT 30. The data was collected using GPES software. The electrochemical cell consisted of a glassy carbon pyrolytic graphite disk (PGE) as working electrode, a platinum wire counter electrode, and a saturated calomel electrode (SCE) as the reference electrode. The immobilization of the freshly prepared Cu^{II}-Rd (10 μL of 2 mM in 50 mM Tris-HCl, pH 7.6) was performed using codeposited neomycin (typically, 2 mg/mL) on the PGE surface. The electrolyte solution consisted of 50 mM Tris-HCl, pH 7.6, 2 mg/mL neomycin sulfate. The modified electrodes were prepared by deposition of an ice-cold protein solution on the freshly polished PGE surface by the solvent casting technique (drying time 30 min at RT) and then cover with 3.5 kDa cutoff membrane. The final configuration is a membrane working electrode with a thin layer of protein. The potentials were corrected and presented in the normal hydrogen reference (NHE) scale.

2.5.4. EPR Studies. X-band EPR (9.65 GHz) spectrum of Cu-Rd frozen solutions (400 μM), at 40K, were recorded using a Bruker EMX 6/1 spectrometer and a dual-mode ER4116DM rectangular cavity (Bruker); the samples were cooled with liquid helium in an Oxford Instruments ESR900 continuous-flow cryostat, fitted with a temperature controller. The acquisition conditions were a modulation frequency of 100 kHz, modulation amplitude of 0.1 mT and a microwave power of 635 μW. The approximate concentration of copper present in the Cu^{II}-Rd samples was determined from the area beneath the integrated spectrum (double integration of the spectrum), using as standard a 2−6 mM Cu^{II}-EDTA solution, in the same buffer system as Rd.

3. RESULTS AND DISCUSSION

3.1. Absorption Spectroscopy and Fluorescence Studies (Aerobic Conditions). Herein we reported two synthesis methods (with and without DTT). In presence of DTT, the initial product is Cu^{I}Rd that further reacts with O_2 to yield Cu^{II}-Rd, whereas in the absent of DTT, the initial product is Cu^{II}-Rd. During reconstitution, the freshly prepared reduced apo-Rd (S−S bonds reduced by DTT followed by dialysis) is incubated with $CuSO_4$ in 1:1 ratio allowing an immediately brown color complex formation, Cu^{II}-Rd, with quantitative yield under aerobic condition due to the high affinity of Cu−thiol interaction. Cu^{II} binding was monitored by UV−visible electronic absorption spectroscopy upon titrating of apo-Rd with increasing amounts of Cu^{II}. At stoichiometric Cu^{II}/apo-Rd ratios, a visible spectrum with bands at 276 nm (ε = 12130 ± 700 M^{-1} cm^{-1}), 355 nm (ε = 3175 ± 150 M^{-1} cm^{-1}), 432 nm (ε = 3450 ± 200 M^{-1} cm^{-1}), 739 nm (ε = 1650 ± 50 M^{-1} cm^{-1}), and a shoulder around 490 nm were observed, saturating at one equivalent of Cu^{II} (Figure 1A). Addition of excess of $CuSO_4$, makes the disappearance of the three visible absorption bands uniformly with time as shown in Figure 1B. Thus, we can conclude that the Cu^{II}-Rd species is susceptible to oxidation by free Cu^{II} ions. Such oxidation is observed for thiol-based reagents[40] and for cysteine residues in other proteins.[41] Under O_2, without excess of Cu^{II} salt, the brown color of Cu^{II}-Rd was also bleached (Figure S1), but the disappearance rate is very slow compared to the obtained by addition of excess Cu^{II} (Figure 1B; inset). This result suggests that Cu^{II}-Rd is reduced to Cu^{I}-Rd which can be recovered in the presence of DTT under O_2 (Figure S2) (cysteine thiol reduced by DTT and Cu^{I} oxidized to Cu^{II} by O_2), indicating that the copper center remains intact. Full recovery is not attained due to the presence of multiple redox systems: Cu, Cys, DTT, and O_2 all act as either internal or external redox active species, whereas internal Cys attempts to reduce the internal Cu^{II}. At the same time, the external O_2 tries to oxidize the internal Cu^{I}, as well as internal Cys, whereas external DTT acts to prevent the Cys oxidation by O_2. The above results show that copper is reduced by Cys and simultaneous formation of a disulfide bond occurs (i.e., Cu−thiol autoreduction).

The reconstitution was also attempted in the presence of DTT (a reducing environment) to attain Cu^{I}-Rd derivative by addition of $CuSO_4$.[31] In this reducing environment, Cu^{II} ion is first reduced by DTT and then coordinated by Cys residues from Rd as a Cu^{I} species. In presence of oxygen from air, the Cu^{I}-Rd is slowly transformed into a Cu^{II}-Rd four coordinated species (Figure 2). Under the described conditions, the copper oxidation process is slow, and the intensity of UV−vis is slightly lower (5−10% with respect to 432 nm) compared with the procedure without DTT (Figure 1) due to minimal external as well as internal redox chemistry (copper and thiol redox-active species). The solution is stable for a longer time scale (Figure 2; inset), meaning that DTT prevents the cysteine oxidation to the Cu^{II}−S−Cys redox system, even in the presence of oxygen (air). When more DTT is added, the stability increases (Figure 2; inset). Generally, addition of Cu^{II} to cysteine rich proteins promotes the disulfide bond formation. We can speculate that Cu^{II} first binds to Cys sulfur to afford Cu^{II}−S−Cys interactions, which decays with time in the presence of O_2 or with excess of Cu^{II} salt. This system is stable under argon with a

DOI: 10.1021/acs.inorgchem.8b00121
Inorg. Chem. 2018, 57, 8078−8088

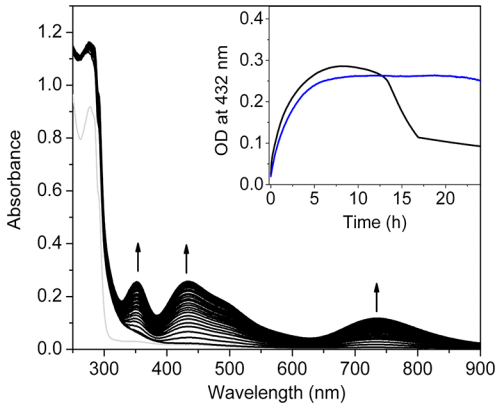

Figure 2. UV−visible spectra of apo-Rd (≈90 μM) with 2 mM DTT followed by addition of $CuSO_4$ (≈90 μM) every 10 min over 6 h (up to saturation of Cu^{II}-Rd formation) in 50 mM Tris-HCl, pH 7.6, at RT. Inset: Comparison oxidation rate of Cu, OD at 432 nm vs time (24 h) in the presence of 1 mM (black) and 2 mM (blue) DTT. Arrows indicate the directions.

1:1 ratio of Cu:Rd (see below). However, the apo-Rd-protein with Cu^{II} is able to prevent this oxidation process, yielding Cu^{II}-Rd with quantitative yield.

The synthesis of Cu^{II}-Rd was also tested with 8 M urea in 50 mM Tris-HCl, pH 7.6, and 50 mM MES buffer, pH 5.5. In basic or in under denaturing conditions, the UV−visible spectra of Cu^{II}-Rd are identical. However, in acidic conditions, the intensity of absorption bands decreases (≈0.5 with respect to 432 nm) (not shown). This implies that protonated cysteine−S has a weaker affinity to Cu^{II}, as expected. Under denaturing conditions, the Cu−S−Cys center is stable since Rd has high resistance to chaotrope-salt effect.[42] Similarly, the small copper-binding protein Azurin recovers spectroscopically the native copper site when adding Cu^{II} to chaotrope-denatured apoprotein.[43]

The UV−visible spectra of Cu^{II}-Rd closely parallel, with distinct absorption features, the Cu^{II}−S−Cys interaction in copper proteins.[44−47] The absorption spectrum of Cu^{II}-Rd is dominated by an intense band at 432 nm (ε = 3450 ± 200 M^{-1} cm^{-1}), compatible with a S(Cys) → Cu σ charge-transfer transition, as in perturbed blue, green, and acoP copper sites.[48] This result suggests that the copper center adopts a distorted tetrahedral geometry and possesses an intense higher energy σ and a weak lower energy π ligand to metal CT transition (σ ground state).[14,16,49] Most Rd derivatives, containing $M-S_4$ cores, adopt a tetrahedral geometry due to the rigid structural framework of protein scaffold that imposes a structure similar to the native one (Fe-center).[32] Reorganization of Cys residues at the coordination site may occur, not being associated with complex protein conformational changes, to generate metal site distorted tetrahedral/tetragonal geometries. The copper binding site in rigid cupredoxins protein matrices allows minor perturbations of the coordinated structure, resulting in a change of geometry, with consequences on the electron transfer properties.[50]

A closer look to the aa sequence of DgRd,[51] indicates the presence of one tryptophan (W) and three tyrosine (Y) near by the coordinating Cys residues ($Y_4XC_6XXC_9XY_{11}XY_{13}$ and $W_{37}XC_{39}XXC_{42}X$). According to the above spectroscopic characterization, $Cu^{II}(Cys)_4$ reduces to $Cu^{I}(Cys)_2$, and one pair of cysteine oxidizes to attain the Cys−S−S−Cys bond formation.

Proteins containing W residues have intrinsic emission properties (fluorescence) that can be used to probe copper oxidation states.[52] We employed time course W fluorescence measurements to probe $Cu^{II/I}$ binding to the rubredoxin during the redox cycle. When excited at either 280 or 295 nm, the aerobically reduced Cu^{I}-Rd system has an emission maximum at ∼333 nm that is typical for protein fluorescence arising primarily from tryptophan (Figure 3B). It is slightly more pronounced when excitation is performed at 295 nm.

Copper proteins containing tyrosines have corresponding absorption bands ranging from ∼308 nm (azurin) to ∼355 nm (e.g., glucagon), quite sensitive to local environment or solvent exposure.[53] The λ_{max} of a buried Y occurs around 335 nm, whereas fully solvent exposed Y has λ_{max} around 355 nm.[53] The Y residue is difficult to detect due to the higher absorptivity coefficient and quantum yield of tryptophan. Quenching studies utilizing intrinsic W fluorescence of proteins can give useful information regarding the Cu^{II} oxidation state. The aerobically reduced stable Cu^{I}-Rd derivatives (after separation of any free metal by PD10) are transformed to Cu^{II}-Rd in the presence of DTT/O_2 over 3 h at RT (Figure 3A). Y intensity is quenched and shifts to lower wavelengths (typically at ∼325 nm), which means that W residues are in different environments (i.e., more buried in a cavity site; Figure 3B). This result indicates that internal geometry at Cu site is rearranged during the redox cycle. The intrinsic fluorescence of W in Rd is decreased upon addition of DTT suggesting reduction of oxidized Cys−S−S−Cys and concomitant oxidation of Cu which quenches the emission of W. Low and Hill[54] demonstrated that reduction

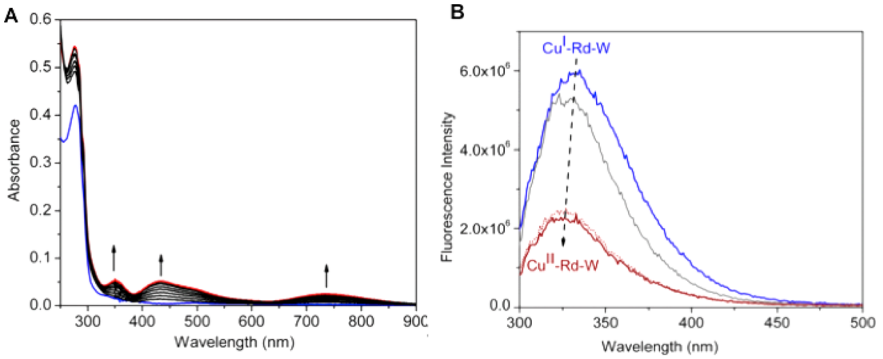

Figure 3. (A) UV−vis of Cu^{I}-Rd (35 μM; blue) with DTT (1 mM) in 50 mM Tris-HCl, pH 7.6, in air at RT every 15 min over 2 h (gray lines); (B) Fluorescence study of tryptophan (W, λ_{exc} = 295 nm) in Cu^{I}-Rd (35 μM) (blue) with 1 mM DTT (2 min; gray) and upon oxidation in air at RT over 2 h (dotted brown) and 3 h (brown). Arrows indicate the directions of intensity.

DOI: 10.1021/acs.inorgchem.8b00121
Inorg. Chem. 2018, 57, 8078−8088

potential of Fe-Rd was fine-tuned by nearby aromatic ring (mediated by iron−sulfur bonds). Therefore, the reduction of copper may be influenced by proximity of residues from Y or W. Y and W both eject electrons upon photochemical irradiation.

3.2. Photolysis and Fluorescence Study (Anoxic Condition). UV−visible results showed that copper is reduced by Cys and fluorescence spectra suggested electron/energy transfer between Cu and W. For confirming this, we performed a set of UV−visible experiments under strict anoxic conditions while simultaneously controlling light exposure.

The fact that the UV−visible spectrum of Cu^{II}-Rd in anoxic (Figure 4) and aerobically conditions are identical, and the

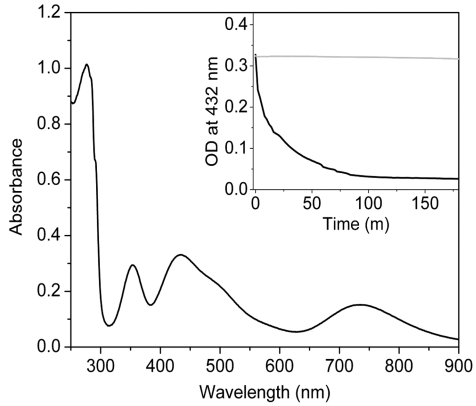

Figure 4. UV−visible of Cu^{II}-Rd (≈90 μM) under anoxic conditions in 50 mM Tris-HCl, pH 7.6, at RT. Inset: OD at 432 nm vs time curve (3 h) of Cu^{II}-Rd with excess $CuSO_4$; 0 equiv (gray) and 2 equiv (black).

observation of a long stability of Cu^{II}-Rd under argon or in the dark (at least 2 days at 4 °C), implies that the Cu−thiol auto reduction mechanism does not apply to the $Cu^{II}S_4$ chromophore. Moreover, the UV−visible spectrum of Cu^{II}-Rd under strict argon atmosphere in the presence of 100 fold excess of DTT does not change or decrease in intensity over 4 h at RT (not shown). Similar redox chemistry is also observed in Cu^{II}-$(S-Cys)_2(Im)(H_2O)$ complex of BsSCO which is not reduced by dithiothreitol.[41] First, under O_2, Cys (one of four residues) is oxidized, which influences the geometry rearrangement at Cu^{II} site to generate an unstable/transient intermediate where Cu^{II} rapidly accept one electron from one of the three Cys to yield $[Cu^{I}(S-Cys)_2 + Cys-S-S-Cys)]$ in the final step (more detailed discussion below). Upon addition of excess of $CuSO_4$ (2 equiv) into the Cu^{II}-Rd solution under anoxic condition, the UV−visible spectra decay with time as shown by OD at 432 nm versus time course (Figure 4; inset). This result confirms that excess of Cu^{II} oxidizes Cys in anoxic conditions resulting in the reduction of Cu^{II}-Rd to Cu^{I}-Rd.

As Cu^{II}-Rd is highly stable under argon or in dark conditions, the Cu^{II}-Rd sample was irradiated through a filter (cut off at 280 nm), under strict argon atmosphere. Figure 5A shows that after 30 min of photolysis, the absorption spectrum almost disappears while the control sample remains unchanged (dark conditions). This result indicates that photochemical reduction occurs providing a more definitive proof of the electron transfer in the photosensitization process. The photolysis experiment of Cu^{II}-Rd carried out in the presence of O_2 showed no influence of O_2 in the copper reduction (not shown).

Solutions were simultaneously analyzed through fluorescence spectroscopy at different irradiation times. Emission intensity increases at around ∼335 nm upon excitation at 280 nm (corresponding to W emission) (Figure 5B), but no Cu−thiolate emission is observed at 500−700 nm ranges (not shown; excited at either 295 or 340 nm). In other copper proteins like azurin, laccase, and stellacyanin, tryptophan emission was also significantly quenched (or enhanced) by the bound Cu^{II} (or Cu^{I}).[55,56]

After photochemical reduction of copper, the reduced sample is incubated with O_2 to allow its reoxidation, but no color was developed. After addition of DTT in the presence of O_2, the UV−visible of Cu^{II}-Rd spectrum appeared (not shown). This result also indicates that Cu^{II} is reduced and Cys is oxidized in this redox process.

Photochemically, W (or Y/F) can also donate electrons and its transfer may involve inter- or intramolecular photochemical pathways.[57,58] For example, light-induced reduction of copper ions can be successfully carried out by direct photolysis in small copper protein, azurin system, and electron transfer occurs from tryptophan to the Cu^{II} center.[59−63] W fluorescence studies in both conditions (aerobic, photoirradiated) provide the same results. We cannot state, however, at this time where the electron comes from (if from Cys or W).

Photoinduced electron transfer and energy transfer both are of critical importance in biology and lead to variations of

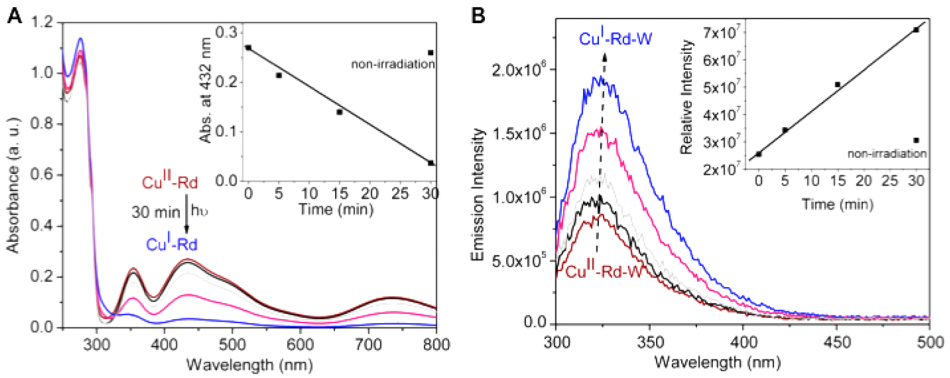

Figure 5. (A) UV−visible spectra of Cu^{II}-Rd (90 μM) with photolysis at 0 min (brown), 5 min (gray), 15 min (purple), and 30 min (blue). A nonirradiated control solution was measured after 30 min (black) in 50 mM Tris-HCl, pH 7.6, at RT; inset: Abs at 432 nm vs photolysis time. (B) Emission spectra of W (λ_{exc} = 295) at 0 min (brown), 5 min (gray), 15 min (purple), and 30 min (blue). A nonirradiated control solution was measured after 30 min (black), insets show the relative emission intensity with photolysis time.

DOI: 10.1021/acs.inorgchem.8b00121
Inorg. Chem. 2018, 57, 8078−8088

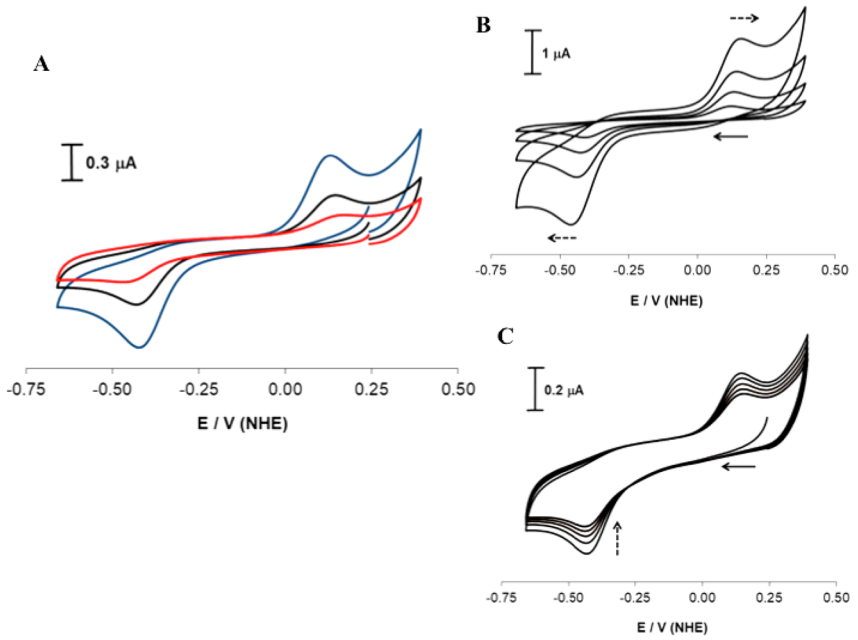

Figure 6. (A) CV of Cu^{II}-Rd (2 mM) in 50 mM Tris-HCl, pH 7.4 at RT; Cu-Rd (blue) with 10 mM NaCl (black) and 20 mM NaCl (red) at scan rate 0.01 V s^{-1}. (B) At different scan rates (0.005, 0.01, 0.02, and 0.05 V s^{-1}) and (C) continuous scan (5 scans) at scan rate 0.01 V s^{-1}. Arrows (full line, black) indicate initial scan direction.

fluorescence emission.[64−66] In the photochemical results, a closer look at ∼280 nm shows that there was no peak intensity change and no shifting of the $\pi-\pi^*$ transition of W.[67] This difference can be related to Cu^{II} and Cu^{I} spectral differences or subtle environment change. Thus, tryptophan may play only energy transfer rather than electron transfer. Photoinduced energy transfer is observed in azurin from *Pseudomonas aeruginosa*,[67,68] where geometry plays a more important role rather than the electron-donating effect, so the geometry may be changed by irradiation (further discussed below).

3.3. Electrochemical Studies. The electrochemical features from the two redox states in Cu-Rd were observed by cyclic voltammetry using the immobilized protein in a thin layer regime. The attained results, namely, the redox peak separation, seem to correlate with possible structural changes, as detailed below. In Figure 6, panel A, we can observe two current peaks at approximately −0.12 V and −0.66 V vs SCE, corresponding to the anodic and cathodic peaks, respectively (anodic peak, E_{pa}, cathodic peak, E_{pc}). Converting the values to the NHE scale, the midpoint potential associated with the process is −0.150 ± 0.004 V vs NHE and the cathodic and anodic peak separation, ΔE_p, is 0.575 ± 0.021 V. The value of these peaks' separation is relatively large, corresponding to the high overpotential associated with the redox transition, suggesting that structural changes may occur during the course of electron transfer, which is expected given the different stereochemical geometry preference for the Cu^{II} and Cu^{I} states in Rd. The cyclic voltammograms were collected at varying scan rates. At higher scan rates, the peak separations are larger, corresponding to an increased irreversibility of the process (Figure 6, panel B). Continuous scanning (Figure 6, panel C) leads to a current intensity decrease at the same peak position, in agreement with a continuous decrease of the electroactivity of the protein. Also, the influence of salts such NaCl was examined. After addition of NaCl aliquots to a Cu-Rd solution, the anodic peak potential is slightly shifted toward positive values (E_{pa} = 0.16 V vs NHE), and the cathodic process shifts slightly to more negative values (E_{pc} = −0.45 V vs NHE), corresponding to a ΔE_p of 0.610 V (Figure 6A, blue). Therefore, the redox potential of copper seems affected by chloride concentration, as expected, because of the known ability of chloride to form strong complexes with copper.[69,70] Both observed processes are codependent, as observed by scanning in different range of potential values and by observing the similar intensities of the currents of the anodic and cathodic peaks. In this chromophore, $Cu^{II}(S-Cys)_4$, both copper and Cys are redox active. During the redox process (from UV−visible studies), the Cu^{II} is reduced and simultaneously Cys is oxidized, so we may infer that this redox cycle involves both centers (Cu and Cys) rather than only one single Cu center. Reduction potentials of Cu^{II}/Cu^{I} in Cu proteins span a large window, modulated by ligand type and coordination geometry (up to 500 mV) when compared to the Cu^{II}/Cu^{I} redox couple in water (+150 mV versus NHE),[16] whereas the redox potential of Cys (no metal bound) in most proteins is ranging from −270 to −125 mV vs NHE.[71,72] It is important to notice that redox potentials are also dependent on the experimental conditions, such as the case of azurin, for instance, that presents values such as +25.8 mV (immobilized on a pyrolytic graphite electrode, pH 8.0, 0.1 M NaCl, scan rate 10 mV/s) found by Alan Bond's group[73] to around +300 mV (immobilized on polymyxin B sulfate modified pyrolytic graphite electrode, pH 8.5, 0.1 M NaCl, scan rate 10 mV/s) found by Hirst and Armstrong.[74] However, the observed midpoint potential of Cu-Rd, $E_{1/2}$ = −0.15 V vs NHE, falls in Cys redox window and may be assigned to one electron oxidation of cysteine in Cu-Rd redox couple which may be proposed as $\{Cu^{II}(S-Cys)_3(Cys-S^*)\}/Cu^{II}(S-Cys)_4$. Interestingly, the oxidized form of the present $\{Cu^{II}(S-Cys)_3(Cys-S^*)\}$ intermediate is very unstable and opens the hypothesis that this is immediately transformed by the decay $\{Cu^{II}(S-Cys)_3(Cys-S^*)\} \rightarrow [Cu^{I}(S-Cys)_2(Cys-S-S-Cys)]$, transferring one electron from Cys to Cu^{II} and manipulating internal geometry resulting in the large separation of cathodic and anodic peak potentials observed. Comparing the observed formal redox

DOI: 10.1021/acs.inorgchem.8b00121
Inorg. Chem. 2018, 57, 8078−8088

potential (−0.150 ± 0.004 V vs NHE) of CuRd, one can observe that although slightly more negative, is close to the range of nonsubstituted rubredoxins (e.g., −0.075 V in Auchére et al.,[75] −0.077 V in Xiao et al.).[76] The more negative result obtained for CuRd indicates an increased reducing ability comparing to other rubredoxins (and also other copper proteins) which seem related with the enhanced stability of the reduced center (CuI state), corroborating the proposed mechanism (see below).

The systems Cu^{II}/Cu^{I} usually present small redox peaks' separations even in biological contexts.[74,77] Large separations such as the obtained (ΔE_p = 0.575 ± 0.021 V) are usually related with mechanisms of ECE type, where a chemical reaction occurs between the two redox reactions (oxidation and reduction) and/or structural changes that imply different (and longer) electronic pathways, increasing the irreversible character of the global reaction and the observed electrochemical behavior (and subsequently increasing the peaks separation), which is also in line with the proposed mechanism (see below). The reduction/oxidation of metal ion in Cu-Rd is tightly related with the structure such as geometric constraints. The structure of the active site plays a key role in the function of the Cu-protein,[50] such as plastocyanin, adopting such an intermediate structure between oxidized and reduced forms ("entatic" or "reduced rack state")[78] leading to fast electron transfer rates since the reorganization energy is small.

3.4. EPR Study. Cu^{II}-Rd gives rise to a characteristic copper EPR signal, with well-resolved hyperfine structure in the $g_{\|}$ region, due to the interaction with one copper nucleus (four lines, from the $I(^{63,65}Cu) = 3/2$) (Figure 7, blue line).

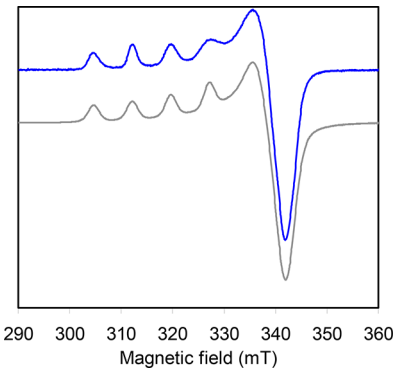

Figure 7. EPR spectrum at 40 K of the Cu-Rd (300−400 μM), in 50 mM Tris-HCl, pH 7.6 (blue line). The signal was simulated (gray line) with $g_{\|,\perp}$ = 2.183 and 2.032 and $A_{\|,\perp} = 76.4 \times 10^{-4}$ and 12×10^{-4} cm^{-1}.

The signal can be simulated with a single Cu^{II}-containing species (d^9 system, $S = 1/2$) with axial symmetry, with $g_{\|,\perp}$ = 2.183 and 2.032 and $A_{\|,\perp} = 76.4 \times 10^{-4}$ and 12×10^{-4} cm^{-1} (Figure 7, gray line). The $g_{\|}$ and $A_{\|}$ values are consistent with a sulfur-rich coordination (if the Peisach−Blumberg correlation for $\{CuS_4\}$ complexes is extrapolated for the low $A_{\|}$ value of Cu-Rd),[79,80] in a distorted tetrahedral structure, as suggested by the high $g_{\|}/A_{\|}$ value of 286 cm,[81] and by the low $A_{\|}$ value.[82,83]

The native iron-containing Rd center has a tetrahedral geometry and several metal-substituted derivatives, other than copper, display a tetrahedral to distorted tetrahedral geometry,[32] thus supporting the *D. gigas* Rd scaffold being able to impose this geometry. Interestingly, the EPR spectrum of the Cu-Rd from *Desulfovibrio vulgaris* Hildenborough suggests a copper center with a structure more close to a square-planar one (higher $A_{\|}$ (119×10^{-4} cm^{-1}) and lower $g_{\|}/A_{\|}$ (183 cm)).[31]

Of note is that the ratio of Rd/Cu used does not change the EPR signal and an identical signal is obtained throughout a Rd titration with 0.66, 1.00, 1.33, and 2.00 mol equiv of copper (data not shown). Moreover, for all those Rd:Cu ratios, the amount of Cu^{II} present is always ≈50% of the copper added, showing that for Rd/Cu from 1.00:0.66 to 1.00:2.00 the final proportion of Cu^{II}/Cu^{I} is always 0.50:0.50. As a hypothesis, these results can be interpreted assuming that some Cys residues in reduced apo-Rd are oxidized in air during isolation process to yield a mixture of monomer (all Cys residues are in reduced form in apo-Rd) and dimer (two Cys are oxidized to yield intermolecular disulfide bond, where one Cys comes from each monomer of reduced apo-Rd) as identified by SDS-PAGE gel (not shown). After addition of Cu^{II} in this mixture system, some amount of Cu^{II} binds with four reduced cysteines (from monomer) to yield Cu^{II}-$(S-Cys)_4$, and some amount of Cu^{II} bind with three reduced cysteins (from dimer) to yield $\{Cu^{II}\text{-}(S-Cys)_3\text{----}Cys-S-S-Cys\text{----}Cu^{II}\text{-}(S-Cys)_3\}$ which is immediately transformed to $2[Cu^{I}\text{-}(S-Cys)_2(Cys-S-S-Cys)]$ but not in the Cu^{II}-$(S-Cys)_4$ system (assumed as very redox unstable).

3.5. Mechanistic Implication of Cu-Rd Redox Cycle. The above results reveal that the mechanism of reduction of Cu^{II} in Cu^{II}-Rd does not follow like the universal Cu−thiol autoredox chemistry. The reduction of copper occurs in two main possible pathways: (i) oxidative and (ii) photochemically.

3.5.1. Reduction of Cu^{II}-Rd: Oxidative Pathway. Thiol residues are oxidized in the presence of molecular oxygen,[84a] and these reactions are catalyzed by copper or iron[40,84b,85] by generating many reactive intermediates such as superoxide anion, hydrogen peroxide, hydroxyl radical, and cysteine radical.[23,40] Therefore, we proposed that under O_2 copper first plays the role of electron carrier from cysteine to oxygen. In this redox process, one out of four Cys in Cu^{II}-Rd is oxidized, and consequently, the molecular O_2 is reduced. The reduction potential associated with the aqueous one electron reduction of O_2 to $O_2^{\bullet-}$ is uphill (−0.16 V vs NHE), while that of the two electrons reduction of O_2 to H_2O_2 is downhill (+0.28 V vs NHE).[86] The midpoint redox potential of Cu-Rd ($E_{1/2}$ = −0.150 V vs NHE) is favorable to reduce O_2 to $O_2^{\bullet-}$. After oxidation of one Cys, the geometry at Cu^{II} site in Cu^{II}-Rd is changed which facilitates to reduce to Cu^{I} by accepting one electron from one of these Cys (three) and concomitant oxidizes Cys. Such oxidation is observed for thiol-based reagents,[40] and for cysteine residues in other copper proteins, BsSCO binds Cu^{II} with ligation by two cysteines, one histidine, and one water.[87,88] Thus, electron donation from each cysteine in each step may be proposed in a radical pathway. We attempted to detect the proposed Cys* radical by using the DMPO as a spin trap agent, but we did not get satisfactorily result. It is a very complex process where Cys, Cu, and O_2 all are redox elements, and all processes are highly dependent and tight regulate to each other. Thus, it is very difficult to detect the particular radical peak in this redox system. It suggested that the rate of S−S bond formation may be faster than the rate of adduct between Cys−S* and DMPO or formation of Cys−S* radical oriented in such a way where the adjacent another Cys−S* radical bind fast rather than DMPO. Due to lack of enough experimental data, we can speculate that areal oxidation of one Cys in Cu^{II}-Rd changed the geometry at Cu^{II} in Cu^{II}-Rd, which facilitates the copper-thiol autoreduction to yield $[Cu^{I}\text{-}(S-Cys)_2$-Rd +

DOI: 10.1021/acs.inorgchem.8b00121
Inorg. Chem. 2018, 57, 8078−8088

Cys−S−S−Cys] (Figure 8). Therefore, geometry at Cu site plays an important role for this redox process.

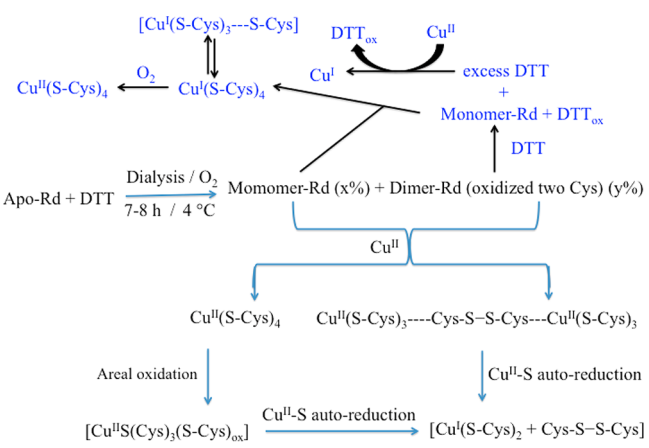

Figure 8. Schematic diagram of the synthesis and probable redox mechanism of Cu-Rd derivative in the presence of DTT and O_2.

Cu protein redox activity is highly influenced by geometry at the Cu site, whereas Fe-Rd is highly influenced by second-sphere amino acid residues (rather than geometry at Fe site) and water molecule at vicinity of active site. In Rd, two cysteines, 6 and 39, are located inside the protein, while cysteines 9 and 42 are surface-exposed. The reduced form reorganized the geometry to open the surface gate Cys_9----Cys_{42} to allow the water molecules to facilitate electron transfer.[89] Therefore, there are two possibilities to formation of S−S bond by intra of intermolecular interaction. Apo-Rd is reduced with DTT, after the dialysis (to remove DTT), further produce a mixture of mono- and dimer of apo-Rd due to the oxidation of two Cys sulfurs (disulfide bond) and one Cys comes from one monomer to yield a dimer (not shown). Therefore, the monomer containing four Cys sulfurs is ready to bind Cu^{II} to yield Cu^{II}-$(S-Cys)_4$-Rd and dimer containing three Cys sulfurs will also bind Cu^{II} but with the three coordinated Cu^{II}-$(S-Cys)_3$-Rd. The latter is unstable which makes it easy to transfer electrons from Cys to Cu^{II} to yield a reduced Cu^{I}-$(S-Cys)_2$-Rd. When DTT is added into this mixture system, the S−S bond in the dimer is cleaved to produce four Cys monomer that bind Cu^{II}, but at the same time, Cu^{II} is reduced to Cu^{I} that will afterward bind to Rd to produce Cu^{I}-Rd. Thus, we get only Cu^{I}-Rd derivatives initially, and after that in the presence of O_2, Cu^{I}-Rd is converted to Cu^{II}-Rd (see UV−visible). Simultaneously, the formation of Cu^{II}-Rd is reduced by oxidizing Cys. The rate of oxidation of copper may be fast comparing to reduction of Cys, resulting that we finally get Cu^{II}-Rd derivatives and not fully $Cu^{II}S_4$Rd system (Figure 8).

The intra- and intermolecular disulfide bond formation mechanisms catalized by metal (Cu, Fe) are found in many biological system, such as human SOD1,[90] human myoglobin,[91] and so on. Allowing S−S bond formation during aerial oxidation of Cys in Cu^{II}-Rd and simultaneously formation of Cu^{I}-Rd occur with different time (t = 0, 1, 3, and 6 h), only one band is observed by SDS−gel (not shown) that is attributed to monomer derivative. It means that intra S−S bond formation can be obtained from two exposed Cys residues, Cys_6 and Cys_{42}. Dimer formation may occur between two Rd by radical formation of Cys, and afterward, fast thiol/disulfide exchanges[92−94] to form intra S−S bond, yielding the monomer. Therefore, apo-Rd oxidation of Cys mainly occurs by intermolecular mechanism, but copper-catalyzed Cys oxidation occurs by intramolecular disulfide bond.[95]

3.5.2. Reduction of Cu^{II}: Photochemically Pathway. In Cu-Rd redox reaction, Cu^{II} is an electron acceptor (A), whereas Cys (or W/Y can supply electron) is an electron donor (D) (Figure 9). Cys is a better electron donor than Y/W/F due to its lower redox potential.[96]

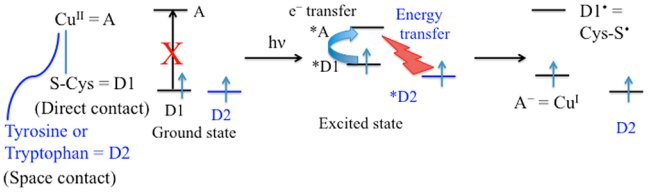

Figure 9. Schematic diagram of photochemically reduction of Cu^{II}-Rd derivative.

The sulfur atom of Cys ligand has three valence 3p orbitals: One p-orbital is used for a carbon−sulfur bond, and the remaining two degenerated p-orbitals that are perpendicular to the S−C bond. Those can interact with the metal center and split in energy depending on C−S−M angle. In Cu proteins, geometry changed from tetrahedral (blue-protein) to tetragonal (red-protein) by changing the C−S−M angle to vary the interaction between S-pπ-orbital and Cu-$d_{x^2-y^2}$ orbital. While interaction is weakening, the maximum absorption peak is shifted to higher energy and vice versa. Therefore, copper proteins can be distinguished on the basis of maximum absorption peak at 400 nm (red-protein; pπ-interaction weak) and 600 nm (blue-protein; pπ-interaction strong).[97] On the basis of UV−visible spectra of Cu^{II}-Rd, the geometry of it is distorted tetrahedral geometry at Cu site with weak pπ-interaction.[44,98] The EPR features suggest that the Cu^{II}-Rd is harboring a distorted tetrahedral metallic center. In biology, stable bis Cys coordinated Cu^{II} complexes exist in BsSCO where the geometry of Cu^{II} site is described as a square pyramidal with weaker S(pπ) → Cu^{II} transitions.[50] The pπ-interaction is weak in Cu^{II}-Rd suggesting the poor overlapping between S-pπ-orbital and Cu-$d_{x^2-y^2}$ orbital. As a result, Cys cannot donate electrons to Cu^{II}-center. Upon photochemical irradiation, the ground-state electrons of Cu^{II}-Rd may be transferred to an electronically excited state and electron addition or removal is easier in the excited state than the ground state[99] resulting in oxidative one-electron transfer from the donor (Cys) excited state to the empty (lower energy) LUMO of a nearby acceptor (Cu^{II}). It indicates that in the ground state of Cu^{II}-Rd orbital overlap between D (Cys) and A (Cu^{II}) is poor, whereas in the excited state, changes in geometry result in Cu−S (covalent interaction) bond formation, which in turn yields a better orbitals overlap between S-pπ and Cu-$d_{x^2-y^2}$ to form a compatible acceptor−donor system (Figure 9).

Photochemically induced electron transfer has been proposed as a mechanism to quench tryptophan fluorescence in a number of proteins, including azurin[62,63,100] where electron transfer occurs from tryptophan to Cu^{II} through the amide backbone[100] or noncovalent interaction by involving other amino acid residues.[101,102] Quenching of fluorescence of a photoexcited molecule can happen in many ways like electron transfer and/or resonance energy transfer. Energy transfer between W and Fe−S cluster in Rd has been observed,[103] also seen in Cu-proteins.[67,68] In this particular case, tryptophan emission is increased as a consequence of Cys being favored as an electron donor, because tryptophan electrons decay radiatively from the excited state to

DOI: 10.1021/acs.inorgchem.8b00121
Inorg. Chem. 2018, 57, 8078−8088

the ground state. At the same time, as Cys is a better electron donor than other amino acid in this system, geometry plays the main role for reduction where "direct-connect" Cys favors the copper reduction rather than "space-contact".

3.5.3. Oxidation of [Cu^{I}(S−Cys)$_2$ + (Cys−S−S−Cys)]: Recycle. The [Cu^{I}(S−Cys)$_2$] + (Cys−S−S−Cys)] is stable in air for long time; thus, the unusual stability of Cu^{I}-complex may be due to the formation of two coordinated inner conformation, Cys$_6$−S−Cu^{I}−S−Cys$_{39}$. The other two solvent-exposed Cys$_9$ and Cys$_{42}$ form disulfide bond that also protects the Cu^{I} system from air by covering the surface. Two coordinate Cys−S−Cu^{I}−S−Cys complexes are found in other sulfur-rich Cu^{I}-proteins, such as Atox1-copper-chaperone[5] as well as partially oxidized yeast Cox17 containing one Cu^{I} diagonally coordinated by two cysteine residues.[104] Therefore, oxidation of [Cu^{I}(S−Cys)$_2$] complex is only possible when changes the coordination at Cu^{I} site opening the surface disulfide gate, Cys$_9$−S−S−Cys$_{42}$ (Figure 10). Reverse reaction, the transformation of

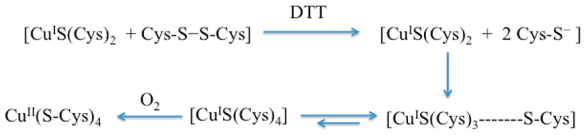

Figure 10. Transformation from Cu^{I}Rd to Cu^{II}-Rd in the presence of DTT + O$_2$ buffer system.

Cu^{I} to Cu^{II} occurs by addition of DTT in the presence of O$_2$. The proposed mechanism is that DTT supply the electron and reductive cleavage the oxidized Cys−S−S−Cys bond to form two free cysteines resulting in opening of the surface gate and allowing the O$_2$ to oxidize Cu^{I} to Cu^{II}. One of the Cys first binds to the Cu^{I}(S−Cys)$_2$ site and pulls the second Cys to generate a transient state, [Cu^{I}(S−Cys)$_4$] ↔ [Cu^{I}(S−Cys)$_3$----(S−Cys)], which is easily oxidized by O$_2$ (the redox potential of Cu-center in transient state may be lower when compared to tricoordinate or bicoordinate Cu^{I}-(S−Cys)$_{2/3}$ resulting in a easy oxidation by O$_2$) to afford a stable Cu^{II}(S−Cys)$_4$ system, completing the redox cycle. When one of Cys is absence in the C$_{42}$A variant, the redox cycle stop here suggesting all four Cys are required to achieve Cu^{II}-state.[31]

Overall, the reduction mechanism at Cu^{II}-center in Cu^{II}-Rd is proposed that the redox chemistry at Cu-center in Cu-Rd is highly influenced by geometry at copper center. In the ground state of Cu^{II}-Rd, Cys cannot supply the electron to Cu^{II} due to poor orbital overlap between Cu and S; when the Cu site is transformed in an intermediate geometry state by excited photochemically or by activated O$_2$ where S-pπ-orbital energetically match with Cu-d$_{x^2-y^2}$ orbital, resulting in better overlapping, then Cys can easily donate an electron to Cu^{II}-center.

4. CONCLUSIONS

We can conclude from this work that the Cu^{II} is reduced by oxidative as well as by a photochemical pathway rather than the universal Cu−thiol autoreduction pathway. The electron transfer from Cys to Cu^{II} is allowed when there is a change in the geometry at the Cu site by induced light or air to form an energetically compatible acceptor−donor system. The redox cycle is off/on by formation of oxidized disulfide bond and reducing cysteine, respectively. Rd-protein scaffold is stabilized in a Cu^{II}S$_4$ chromophore by coordinating four Cys ligands with modest degree of pπ-interaction, which provides poor electronic coupling between donor and acceptor in electron transfer. This feature is different from cupredoxins (one Cys) with a high degree of Cu−S covalency but similar to Cu^{II}−BSco site (two Cys). This model can find the limit of electronic structure as well as electron transfer properties of a mononuclear Cu^{II} system by increasing the Cys ligation at mononuclear Cu^{II} site. However, Nature has not yet utilized this mononuclear Cu^{II}S$_4$ site in current known metalloproteins. Generally, in biology, copper-cofactors act as ET transfer devices (i.e., azurins), catalytic redox active centers (i.e., nitrous oxide reductases, Cu-nitrite reductases) or copper transporter (i.e., Atox1). In the redox-active copper cofactor, copper has two stable redox states, Cu^{I}/Cu^{II} with permanently coordinated states, that changes oxidation states reversibly during catalysis and electron transfer processes. According to the needs of the catalyzed reaction, nature has created different systems, which are mainly coordinated by N-, O-, and S-donor canonical amino acid side chain. However, copper trafficking pathway, Cu transfer is involved by changing the coordination number at Cu site, and the Cu^{I}Cys$_2$ (Atox1) site can easily transfer the Cu to target copper-proteins. The Cu^{II}-Rd has two stable oxidation states; Cu^{II} (higher coordination number) and Cu^{I} (lower coordination number) show a large separation of cathodic and anodic peaks potential (ΔE = 0.575 V). From this redox behavior, Cu^{II}S$_4$ site cannot be suitable for fast electron transfer process like copper proteins. In contrast, in the presence of molecular O$_2$, Cu^{II}−Cys$_4$ is reduced to Cu^{I} with low-coordination site which may play as a copper transfer protein but in this redox process may produce lot of harmful radicals like superoxide, hydroxyl radical, and cysteine radical that may damage the biomolecules. From these reasons, Nature may not use Cu^{II}−Cys$_4$ as ET devices or copper transporters. Finally, this system may function as a redox switch like Sco1 (or BSco), which is an essential accessory protein for CuA assembly in which oxidation of two Cys residues in the Cu^{II} binding may facilitate Cu^{I} transfer.

■ ASSOCIATED CONTENT

Supporting Information

The Supporting Information is available free of charge on the ACS Publications website at DOI: 10.1021/acs.inorgchem.8b00121.

UV−visible spectra of Cu^{II}-Rd under O$_2$ and of recycling between Cu^{II}-Rd to Cu^{I}-Rd (PDF)

■ AUTHOR INFORMATION

Corresponding Author

*E-mail: jose.moura@fct.unl.pt.

ORCID

Luisa B. Maia: 0000-0002-6901-6591
Artur J. Moro: 0000-0003-3285-4919
João C. Lima: 0000-0003-0528-1967
Cristina M. Cordas: 0000-0002-7892-8955
Isabel Moura: 0000-0003-0971-4977
José J. G. Moura: 0000-0002-4726-2388

Notes

The authors declare no competing financial interest.

■ ACKNOWLEDGMENTS

This work was supported by the Associate Laboratory Research Unit for Green Chemistry−Technologies and Processes Clean (LAQV), financed by national funds from FCT/MEC (UID/QUI/50006/2013) and cofinanced by the ERDF under the

DOI: 10.1021/acs.inorgchem.8b00121
Inorg. Chem. 2018, 57, 8078−8088

PT2020 Partnership Agreement (POCI-01-0145-FEDER-007265). B.K.M. thanks UCIBIO, REQUIMTE, for the postdoctoral fellowship grant (UCIBIO-REQUIMTE/013/2016). A.J.M. thanks LAQV-REQUIMTE for the postdoctoral fellowship (LAQV/BPD/002/2017). L.B.M. thanks FCT/MCTES for the postdoctoral fellowship grant (SFRH/BPD/111404/2015), which are financed by national funds and cofinanced by FSE.

REFERENCES

(1) Stiefel, E. I. Transition Metal Sulfur Chemistry: Biological and Industrial Significance and Key Trends. *Transition Metal Sulfur Chemistry*. **1996**, *653*, 2−38.
(2) Belle, C.; Rammal, W.; Pierre, J.-L. *J. Inorg. Biochem.* **2005**, *99* (10), 1929−1936.
(3) Solomon, E. I.; et al. *Chem. Rev.* **2014**, *114* (7), 3659−3853.
(4) Kim, B.-E.; Nevitt, T.; Thiele, D. J. *Nat. Chem. Biol.* **2008**, *4* (3), 176−185.
(5) Boal, A. K.; Rosenzweig, A. C. *Chem. Rev.* **2009**, *109* (10), 4760−4779.
(6) Robinson, N. J.; Winge, D. R. *Annu. Rev. Biochem.* **2010**, *79* (1), 537−562.
(7) Morgada, M. N.; et al. *Proc. Natl. Acad. Sci. U. S. A.* **2015**, *112* (38), 11771−11776.
(8) Iwata, S.; et al. *Nature* **1995**, *376* (6542), 660−669.
(9) Hong-Hermesdorf, A.; et al. *Nat. Chem. Biol.* **2014**, *10* (12), 1034−1042.
(10) Banci, L.; et al. *Proc. Natl. Acad. Sci. U. S. A.* **2008**, *105* (19), 6803−6808.
(11) Rubino, J. T.; Franz, K. J. *J. Inorg. Biochem.* **2012**, *107* (1), 129−143.
(12) Lamb, A. L.; et al. *Nat. Struct. Biol.* **2001**, *8* (9), 751−755.
(13) Ye, Q.; et al. *Biochemistry* **2005**, *44* (8), 2934−2942.
(14) Solomon, E. I. *Inorg. Chem.* **2006**, *45* (20), 8012−8025.
(15) Szilagyi, R. K.; Solomon, E. I. *Curr. Opin. Chem. Biol.* **2002**, *6* (2), 250−258.
(16) Solomon, E. I.; et al. *Chem. Rev.* **2004**, *104* (2), 419−458.
(17) Zaballa, M.-E.; et al. *Proc. Natl. Acad. Sci. U. S. A.* **2012**, *109* (24), 9254−9259.
(18) Cawthorn, T. R.; et al. *Biochemistry* **2009**, *48* (21), 4448−4454.
(19) Glerum, D. M.; Shtanko, A.; Tzagoloff, A. *J. Biol. Chem.* **1996**, *271* (34), 20531−20535.
(20) Meloni, G.; Faller, P.; Vašák, M. *J. Biol. Chem.* **2007**, *282* (22), 16068−16078.
(21) Finkel, T.; Holbrook, N. J. *Nature* **2000**, *408* (6809), 239−247.
(22) Garai, K.; et al. *Biochemistry* **2007**, *46* (37), 10655−10663.
(23) Gaggelli, E.; et al. *Chem. Rev.* **2006**, *106* (6), 1995−2044.
(24) Hemmerich, P.; Beinert, H.; Vänngard, T. *Angew. Chem., Int. Ed. Engl.* **1966**, *5* (4), 422−423.
(25) Rigo, A.; et al. *J. Inorg. Biochem.* **2004**, *98* (9), 1495−1501.
(26) Blumberg, W. E.; Peisach, J. *J. Chem. Phys.* **1968**, *49* (4), 1793−1802.
(27) Klotz, I. M.; Czerlinski, G. H.; Fiess, H. A. *J. Am. Chem. Soc.* **1958**, *80* (12), 2920−2923.
(28) Baek, H. K.; Cooper, R. L.; Holwerda, R. A. *Inorg. Chem.* **1985**, *24* (7), 1077−1081.
(29) Anderson, C. H.; Holwerda, R. A. *J. Inorg. Biochem.* **1984**, *23* (1), 29−41.
(30) Aliaga, M. E.; Andrade-Acuña, D.; López-Alarcón, C.; Sandoval-Acuña, C.; Speisky, H.; et al. *J. Inorg. Biochem.* **2013**, *129*, 119−126.
(31) Thapper, A.; Rizzi, A. C.; Brondino, C. D.; Wedd, A. G.; Pais, R. J.; Maiti, B. K.; Moura, I.; Pauleta, S. R.; Moura, J. J. G.; et al. *J. Inorg. Biochem.* **2013**, *127*, 232−237.
(32) Maiti, B. K.; Almeida, R. M.; Moura, I.; Moura, J. J. G.; et al. *Coord. Chem. Rev.* **2017**, *352*, 379−397.
(33) Maiti, B. K.; et al. *JBIC, J. Biol. Inorg. Chem.* **2015**, *20* (5), 821−829.
(34) Saint-Martin, P.; et al. *Proc. Natl. Acad. Sci. U. S. A.* **1988**, *85* (24), 9378−9380.
(35) Almeida, R. M.; et al. *J. Inorg. Biochem.* **2009**, *103* (9), 1245−1253.
(36) Moura, I.; et al. *Biochem. Biophys. Res. Commun.* **1977**, *75* (4), 1037−1044.
(37) Bruschi, M.; Hatchikian, C. E.; Golovleva, L. A.; Gall, J. L. *J. Bacteriol.* **1977**, *129* (1), 30−38.
(38) Lode, E. T.; Coon, M. J. *J. Biol. Chem.* **1971**, *246* (3), 791−802.
(39) Lowry, O. H.; Rosebrough, N. J.; Farr, A. L.; Randall, R. J. *J. Biol. Chem.* **1951**, *193* (1), 265−275.
(40) Kachur, A. V.; Koch, C. J.; Biaglow, J. E. *Free Radical Res.* **1999**, *31* (1), 23−34.
(41) Hill, B. C.; Andrews, D. *Biochim. Biophys. Acta, Bioenerg.* **2012**, *1817* (6), 948−954.
(42) Morleo, A.; et al. *Biochemistry* **2010**, *49* (31), 6627−6634.
(43) Wilson, C. J.; Apiyo, D.; Wittung-Stafshede, P. *Q. Rev. Biophys.* **2004**, *37* (3−4), 285−314.
(44) Arciero, D. M.; et al. *Biochemistry* **2002**, *41* (6), 1703−1709.
(45) Gewirth, A. A.; Solomon, E. I. *J. Am. Chem. Soc.* **1988**, *110* (12), 3811−3819.
(46) Lu, Y.; et al. *J. Am. Chem. Soc.* **1993**, *115* (14), 5907−5918.
(47) Wilson, T. D.; Yu, Y.; Lu, Y. *Coord. Chem. Rev.* **2013**, *257* (1), 260−276.
(48) Roger, M.; et al. *PLoS One* **2014**, *9* (6), e98941.
(49) Ghosh, S.; et al. *Proc. Natl. Acad. Sci. U. S. A.* **2009**, *106* (13), 4969−4974.
(50) Siluvai, G. S.; et al. *J. Am. Chem. Soc.* **2010**, *132* (14), 5215−5226.
(51) Hormel, S.; et al. *FEBS Lett.* **1986**, *201* (1), 147−150.
(52) Truong, K.; Ikura, M. *Curr. Opin. Struct. Biol.* **2001**, *11* (5), 573−578.
(53) Vivian, J. T.; Callis, P. R. *Biophys. J.* **2001**, *80* (5), 2093−2109.
(54) Low, D. W.; Hill, M. G. *J. Am. Chem. Soc.* **1998**, *120* (44), 11536−11537.
(55) Larson, B. C.; et al. *J. Phys. Chem. B* **2015**, *119* (29), 9438−9449.
(56) Goldberg, M.; Pecht, I. *Proc. Natl. Acad. Sci. U. S. A.* **1974**, *71* (12), 4684−4687.
(57) Bent, D. V.; Hayon, E. *J. Am. Chem. Soc.* **1975**, *97* (10), 2612−2619.
(58) Mialocq, J. C.; et al. *J. Phys. Chem.* **1982**, *86* (16), 3173−3177.
(59) Shafaat, H. S.; et al. *J. Am. Chem. Soc.* **2010**, *132* (26), 9030−9039.
(60) Kroes, S. J.; et al. *Biophys. J.* **1998**, *75* (5), 2441−2450.
(61) Gilardi, G.; et al. *Biochemistry* **1994**, *33* (6), 1425−1432.
(62) Petrich, J. W.; Longworth, J. W.; Fleming, G. R. *Biochemistry* **1987**, *26* (10), 2711−2722.
(63) Hansen, J. E.; Longworth, J. W.; Fleming, G. R. *Biochemistry* **1990**, *29* (31), 7329−7338.
(64) Huber, R. *Angew. Chem., Int. Ed. Engl.* **1989**, *28* (7), 848−869.
(65) Winkler, J. R.; Gray, H. B. *Chem. Rev.* **2014**, *114* (7), 3369−3380.
(66) Doose, S.; Neuweiler, H.; Sauer, M. *ChemPhysChem* **2009**, *10* (9−10), 1389−1398.
(67) Sweeney, J. A.; et al. *J. Am. Chem. Soc.* **1991**, *113* (20), 7531−7537.
(68) Tobin, P. H.; Wilson, C. J. *J. Am. Chem. Soc.* **2014**, *136* (5), 1793−1802.
(69) Fritz, J. J. *J. Phys. Chem.* **1980**, *84* (18), 2241−2246.
(70) Zhao, H.; et al. *Anal. Chem.* **2013**, *85* (16), 7696−7703.
(71) Nishinaka, Y.; et al. *Redox Rep.* **2001**, *6* (5), 289−295.
(72) Collet, J.-F.; Bardwell, J. C. A. *Mol. Microbiol.* **2002**, *44* (1), 1−8.
(73) Guo, S.; et al. *Anal. Chem.* **2004**, *76* (1), 166−177.
(74) Hirst, J.; Armstrong, F. A. *Anal. Chem.* **1998**, *70* (23), 5062−5071.
(75) Auchère, F.; et al. *JBIC, J. Biol. Inorg. Chem.* **2004**, *9* (7), 839−849.

DOI: 10.1021/acs.inorgchem.8b00121
Inorg. Chem. 2018, 57, 8078−8088

(76) Xiao, Z.; et al. *JBIC, J. Biol. Inorg. Chem.* **2000**, *5* (1), 75−84.
(77) Armstrong, F. A.; Heering, H. A.; Hirst, J. *Chem. Soc. Rev.* **1997**, *26* (3), 169−179.
(78) Solomon, E. I.; Hadt, R. G. *Coord. Chem. Rev.* **2011**, *255* (7), 774−789.
(79) Peisach, J.; Blumberg, W. E. *Arch. Biochem. Biophys.* **1974**, *165* (2), 691−708.
(80) Hoffmann, S. K.; Goslar, J.; Lijewski, S.; Zalewska, A. *J. Magn. Reson.* **2013**, *236*, 7−14.
(81) Tetrahedral distortion increases $g_{\|}$ and decreases $A_{\|}$ values, for S-, N-, and O-donor ligands, being an effective source of reduction of the $A_{\|}$ values: Yokoi, H.; Addison, A. W. *Inorg. Chem.* **1977**, *16*, 1341. Sakaguchi, U.; Addison, A. W. *J. Chem. Soc., Dalton Trans.* **1979**, 600. Hence, the ratio $g_{\|}/A_{\|}$ can be used as an empirical parameter of distortion of the donor set from planar toward tetrahedral geometry: square-planar structures display values of 105−135 cm^{-1}, while higher values (220−700 cm^{-1}) suggest significant tetrahedral distortion.
(82) Square-planar compounds tend to have $A_{\|} > 140 \times 10^{-4}$ cm^{-1}, even with four sulfur ligands. Sakaguchi, U.; Addison, A. W. *J. Chem. Soc., Dalton Trans.* **1979**, 600.
(83) Maiti, B. K.; et al. *Inorg. Chem.* **2014**, *53* (24), 12799−12808.
(84) (a) Mathews, A. P.; Walker, S. *J. Biol. Chem.* **1909**, *6*, 21−28, (b) 299−312.
(85) Pecci, L.; et al. *Amino Acids* **1997**, *13* (3), 355−367.
(86) Wood, P. M. *Biochem. J.* **1988**, *253* (1), 287.
(87) Imriskova-Sosova, I.; et al. *Biochemistry* **2005**, *44* (51), 16949−16956.
(88) Andruzzi, L.; et al. *J. Am. Chem. Soc.* **2005**, *127* (47), 16548−16558.
(89) Min, T.; et al. *Protein Sci.* **2001**, *10* (3), 613−621.
(90) Bouldin, S. D.; Darch, M. A.; Hart, P. J.; Outten, C. E. *Biochem. J.* **2012**, *446* (1), 59−67.
(91) Witting, P. K.; Mauk, A. G. *J. Biol. Chem.* **2001**, *276* (19), 16540−16547.
(92) Jacob, C.; et al. *Angew. Chem., Int. Ed.* **2003**, *42* (39), 4742−4758.
(93) Rombouts, I.; Lagrain, B.; Scherf, K. A.; Lambrecht, M. A.; Koehler, P.; Delcour, J. A. *Sci. Rep.* **2015**, *5*, 12210.
(94) Trivedi, M.; Laurence, J.; Siahaan, T. *Curr. Protein Pept. Sci.* **2009**, *10* (6), 614−625.
(95) Prudent, M.; Girault, H. H. *Metallomics* **2009**, *1* (2), 157−165.
(96) Harriman, A. *J. Phys. Chem.* **1987**, *91* (24), 6102−6104.
(97) Chacón, K. N.; Blackburn, N. J. *J. Am. Chem. Soc.* **2012**, *134* (39), 16401−16412.
(98) Basumallick, L.; et al. *J. Am. Chem. Soc.* **2005**, *127* (10), 3531−3544.
(99) Kavarnos, G. J.; Turro, N. J. *Chem. Rev.* **1986**, *86* (2), 401−449.
(100) Callis, P. R.; Liu, T. *J. Phys. Chem. B* **2004**, *108* (14), 4248−4259.
(101) Okada, A.; Miura, T.; Takeuchi, H. *Biochemistry* **2001**, *40* (20), 6053−6060.
(102) Xue, Y.; et al. *Nat. Chem. Biol.* **2008**, *4* (2), 107−109.
(103) Zhong, D.; et al. *Proc. Natl. Acad. Sci. U. S. A.* **2002**, *99* (1), 13−18.
(104) Arnesano, F.; et al. *Structure* **2005**, *13* (5), 713−722.

DOI: 10.1021/acs.inorgchem.8b00121
Inorg. Chem. 2018, 57, 8078−8088